Bulletin of the Seismological Society of America, Vol. 104, No. 1, pp. 560–566, February 2014, doi: 10.1785/0120130140

Ⓔ

Short Note

Lack of Spatiotemporal Localization of Foreshocks before the 1999 M_w 7.1 Düzce, Turkey, Earthquake

by Chunquan Wu, Xiaofeng Meng, Zhigang Peng, and Yehuda Ben-Zion

Abstract We use a matched-filter technique to detect small seismic events before the M_w 7.1 Düzce earthquake that are not included in the regular catalog. The study employs extensive waveform dataset recorded by a 10-station fault zone array near the epicenter of the Düzce earthquake, deployed about three months before the event. We use 3134 earthquakes within 20 km of the Düzce epicenter listed in the local catalog as templates to scan through waveforms recorded within ∼65 hours before the Düzce earthquake. The analysis reveals 262 newly detected events in this time interval, which is ∼5 times more than the 55 events listed in the original catalog. Most of the events occur to the west of the Düzce epicenter, which was initiated between a more active western and relatively quite eastern fault segments. The results do not indicate a localizing foreshock process that accelerates in time and/or involves progressive concentration of activity around the mainshock hypocenter during the preceding 65 hour period. Instead, we find that the Düzce source region becomes less active during the ∼20 hours immediately before the mainshock. Our results, together with other recent studies, suggest that progressive acceleration and localization of foreshocks around the mainshock epicenter is not a general phenomenon.

Online Material: Figures of timing of recorded waveforms, peak ground velocities, foreshock activity, seismicity rate, and temporal evolution of earthquake activity, vertical waveforms, and distribution of template events.

Introduction

Reliable high-resolution observations of foreshock patterns can provide fundamental information on earthquake physics and may lead to improved strategies for earthquake prediction (e.g., Jones and Molnar, 1979; Dodge *et al.*, 1995, 1996; Ben-Zion, 2008). Only about half of the well-recorded large earthquakes are preceded in standard catalogs by at least one foreshock (Abercrombie and Mori, 1996). Recent detailed analysis of seismicity clusters in southern California indicates a variety of patterns associated with different types of foreshocks–mainshock–aftershocks sequences (Zaliapin and Ben-Zion, 2013a,b). However, high-resolution recordings near the hypocenters of large events may, in principle, contain simpler and more universal patterns.

During 1999, two large earthquakes occurred along the North Anatolian fault (NAF) in northwestern Turkey. On 17 August, the M_w 7.4 Izmit earthquake ruptured the NAF along a 125 km segment, from the Sea of Marmara in the west toward Düzce in the east. About three months later, the 12 November M_w 7.1 Düzce earthquake ruptured slightly back to the west and about 50 km further to the east (Fig. 1). These two earthquakes were the latest in a sequence of large events that ruptured ∼1000 km off the NAF since 1939 (Ozalaybey *et al.*, 2002).

Bouchon *et al.* (2011) observed a remarkable sequence of foreshocks in close proximity to the hypocenter of the Izmit earthquake. This sequence consists of about 18 foreshocks with very similar waveforms and reducing recurrence intervals in the last hour before the Izmit mainshock. The results were interpreted to reflect a phase of accelerating slow slip at the base of the brittle crust before the Izmit earthquake. Kato *et al.* (2012) analyzed the foreshock activities before the recent M_w 9.0 Tohoku-Oki earthquake in Japan. They observed two distinct phases of foreshock migration, which suggested two sequences of slow slip transients propagating to the initiation point of the Tohoku-Oki earthquake. Recently Chen and Shearer (2013) found that the foreshocks of three **M** ∼ 7 earthquakes in southern California have lower stress drops than the aftershocks of these events, suggesting they may be driven by aseismic transients like earthquake swarms.

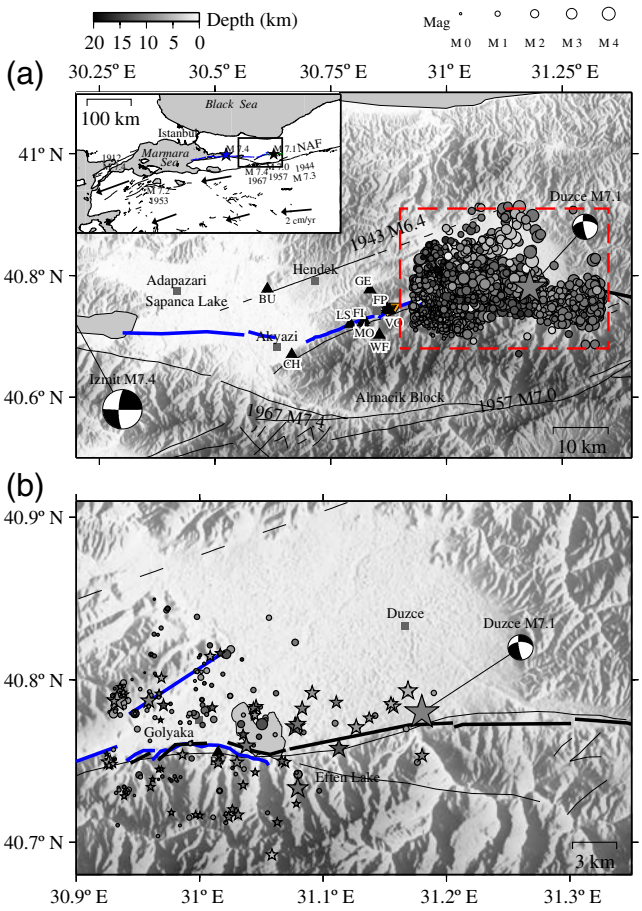

Figure 1. (a) Topographic map of the area along the Karadere–Düzce branch of the North Anatolian fault (NAF). Circles mark the locations of 3134 template events. The large star marks the location of the Düzce earthquake with the moment tensor solution nearby. Shaded background indicates topography, with white being low and dark being high. The surface ruptures of the Izmit and Düzce earthquakes are indicated with thick lines. Dark thin lines associated with earthquake information denote faults that were active during recent ruptures. The locations of the 10 stations in the temporary array and the four stations used in Bouchon and Karabulut (2002) are marked as triangles and inverted triangles, respectively. Squares denote locations of nearby cities. The area bounded by the dashed lines is shown in (b). The inset illustrates the tectonic environment in northwestern Turkey, with the box corresponding to our study area. Vectors represent plate deformation rate. (b) A zoom-in map around the Düzce epicenter showing only the seismic events within the last 65 hours listed in the catalog (stars) and detected in this study (circles). All other symbols are the same as in (a). The color version of this figure is available only in the electronic edition.

It is still not clear how often accelerated foreshock activity occurs before large earthquakes. For example, such behavior was not observed before the 2008 M_w 6.9 Iwate–Miyagi inland earthquake in Japan (Doi and Kawakata, 2012) and the 2010 M_w 6.9 Yushu earthquake in China (Peng *et al.*, 2013). Like aftershocks or earthquake swarms, foreshocks generally occurred close in space and time (Zaliapin and Ben-Zion, 2013a,b). Hence, sometimes standard event detection algorithms may not completely capture foreshocks with smaller magnitudes (Zanzerkia *et al.*, 2003). It is important to identify potentially missing foreshocks for improved understanding of the foreshock patterns and physical mechanisms.

Bouchon and Karabulut (2002) found the 1999 M_w 7.1 Düzce earthquake, which occurred three months after the Izmit earthquake, was preceded by six foreshocks within about five hours before the mainshock. However, these foreshocks are not located due to limited station coverage (Bouchon and Karabulut, 2002), and only the largest one of the six foreshocks is listed in a local catalog based on a 10-station seismic network near the hypocenter of the Düzce earthquake (Seeber *et al.*, 2000). Here we apply the waveform matched-filter technique (Peng and Zhao, 2009) to detect missing foreshocks recorded by this 10-station network. Our dataset in close space–time proximity to the Düzce hypocenter provides a good opportunity for investigating the detailed evolution of foreshock activity before the Düzce mainshock.

Data and Analysis Procedure

Seismic Data

The analysis employs primarily weak-motion data recorded in triggered mode by a temporary 10-station PASSCAL seismic network (Fig. 1) deployed along and around the Karadere–Düzce branch of the NAF a week after the 17 August 1999 M_w 7.4 Izmit earthquake (Seeber *et al.*, 2000; Ben-Zion *et al.*, 2003). All 10 stations had RefTek recorders and three-component L22 short-period sensors with a sampling frequency of 100 Hz. In addition, eight stations had three-component force-balance accelerometers. Within the six month operational period, this network recorded seismograms of ~26,000 earthquakes detected with standard techniques. These include the 12 November 1999 M_w 7.1 Düzce mainshock and its potential foreshocks and aftershocks. During the 65 hour period before the Düzce mainshock, the network recorded ~6000 individual three-component waveforms (Ⓔ Fig. S1, available in the electronic supplement to this article). A total of 55 events were listed in the local catalog (Seeber *et al.*, 2000). Additional details regarding the seismic experiment and dataset are given by Seeber *et al.* (2000) and Ben-Zion *et al.* (2003).

Analysis Procedure

The analysis procedure generally follows that of Peng and Zhao (2009) and is briefly described here. We first select 3143 earthquakes within 20 km of the epicenter of the Düzce mainshock from the local catalog (Seeber *et al.*, 2000) as template events. These include both events that occurred before and after the Düzce mainshock (from August 1999 to February 2000). Because the target waveforms are recorded in triggered mode, we match the beginning time of the recordings from different stations and put all the recordings that start within 10 s into a set of target waveforms.

We require a set of target waveforms within the last 65 hours before the Düzce mainshock to have at least 12 waveforms (or four stations). We end up with 517 sets of target waveforms within 65 hours before the Düzce mainshock, which include ~3700 three-component waveforms. A two-way fourth-order 2–16 Hz Butterworth filter is applied to both the template and target waveforms. Next, we cut 1 s before to 3 s after the *P*-wave arrival at the vertical component of the template waveforms as the *P*-window templates and 1 s before to 3 s after *S*-wave arrival at the east and north components of the template waveforms as the *S*-window templates. We compute the sliding-window cross-correlation functions between the *P*-window template and the vertical component of the target waveforms and between the *S*-window templates and the east and north components of the target waveforms, respectively.

Next, the waveform cross-correlation functions from different components and stations between a template and target event pair are shifted back to the origin time of the template event and then are stacked together to obtain a mean waveform cross-correlation function. We require there to be at least nine cross-correlation functions (or three stations) to ensure the significance of stacking, and we allow one data point shift to ensure the cross-correlation functions from different components and stations are matched correctly (Meng *et al.*, 2013). Finally we identify the points with correlation coefficient (CC) values larger than nine times the median absolute deviation (MAD) in the mean waveform cross-correlation function as positive detections. For a normally distributed random variable, the probability of exceeding nine times MAD is $\sim 6.4 \times 10^{-10}$, so the chance of random detection is quite low (e.g., Shelly *et al.*, 2007; Peng and Zhao, 2009). Figure 2 shows a positive detection at 04:16:55, 12 November 1999, about 13 hours before the Düzce mainshock. This detection has a mean CC value of 0.92, well above the threshold of 0.19. This event was not listed in the local catalog.

If the waveforms recorded at multiple stations are very similar between the template and target events, they should have very close hypocentral locations. As done before (e.g., Peng and Zhao, 2009), we assign the hypocentral locations of the template events to the detected events, and the time with the highest mean CC value as the origin time of the detected events. Then we compute the magnitude of the detected event from the magnitude of the template event and the median value of the maximum amplitude ratios for all channels between the template and detected events, assuming a tenfold increase in amplitude corresponds to one unit increase in magnitude (Peng and Zhao, 2009). For a target event detected by multiple template events, we use the template event with the highest CC value to obtain the location, origin time, and magnitude of the target event (Meng *et al.*, 2013).

Results

Applying the procedure described in Analysis Procedure section leads to detection of 262 earthquakes in the 65 hour period before the Düzce earthquake (Fig. 3a), which is ~5 times more than the 55 earthquakes listed in the local catalog (Seeber *et al.*, 2000). The estimated magnitudes of the detected earthquakes range from −1.1 to 3.1 with 95% of the events having magnitudes less than 2 (Fig. 3b). Most of the detected earthquakes (~98%) occur along the fault segment to the west of the Düzce epicenter (Fig. 1b), whereas the segment to the east of the Düzce epicenter has only ~2% of the detected events. The depths of the detected events are in the range of ~1–15 km (Fig. 4). The earthquakes along the NAF to the west of the Düzce epicenter are generally in the depth range of ~5–10 km, with several exceptions at a depth of ~15 km near the immediate vicinity of the Düzce epicenter. There is not much seismicity in the Almacik block to the

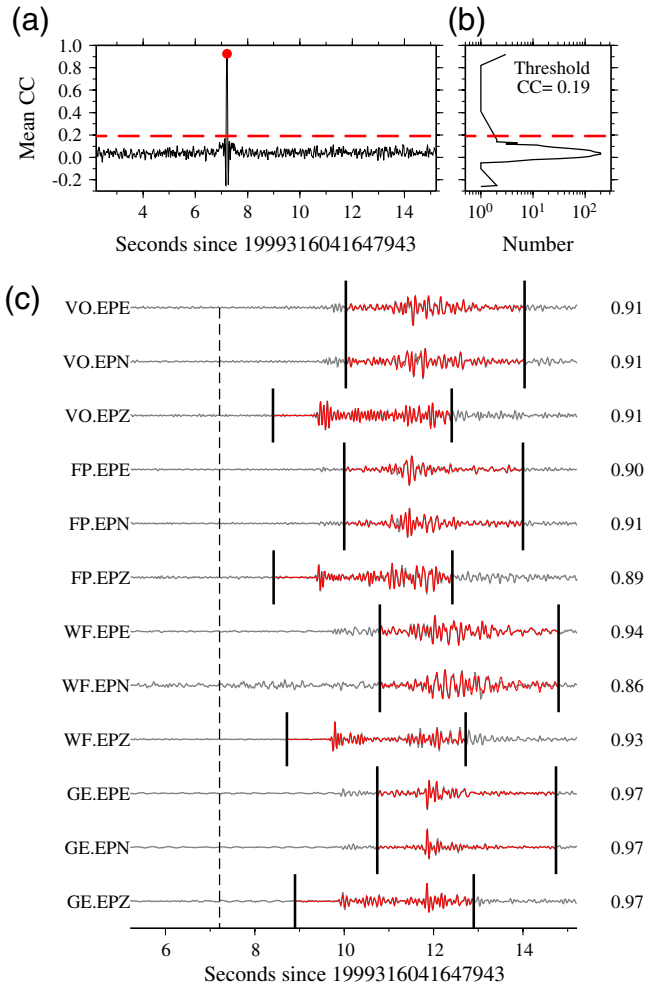

Figure 2. An example of newly detected foreshock of Düzce earthquake. (a) Mean correlation coefficient trace versus time for a template event occurred at 23:29:53, 11 November 1999. The dot corresponds to the detected event at ~5 s after the beginning time of the target waveform recorded at 04:16:55, 11 December 1999. (b) The mean CC function. (c) A comparison of the template waveforms and the target waveforms around the origin time of detected event (vertical dashed line). The station, channel names, and the corresponding CC values are labeled on the left and right sides, respectively. The color version of this figure is available only in the electronic edition.

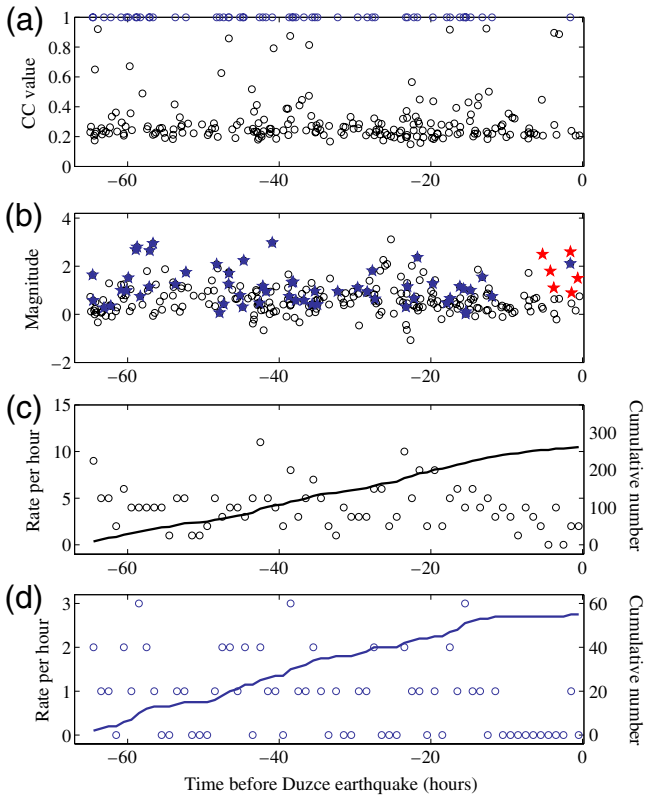

Figure 3. Comparison of the newly detected foreshocks and the foreshocks listed in the catalog. (a) The CC values versus the origin times of all detected events. The circles and stars show newly detected foreshocks and the foreshocks listed in the catalog, respectively. (b) The magnitudes versus the origin times of newly detected events (circles), earthquakes listed in the catalog (open stars), and the six foreshocks (solid stars) found in Bouchon and Karabulut (2002), respectively. (c) The circles denote hourly seismicity rate of the detected foreshocks, and the curve shows cumulative number of detected foreshocks. (d) Similar plot as (c) for the foreshocks listed in the catalog. The color version of this figure is available only in the electronic edition.

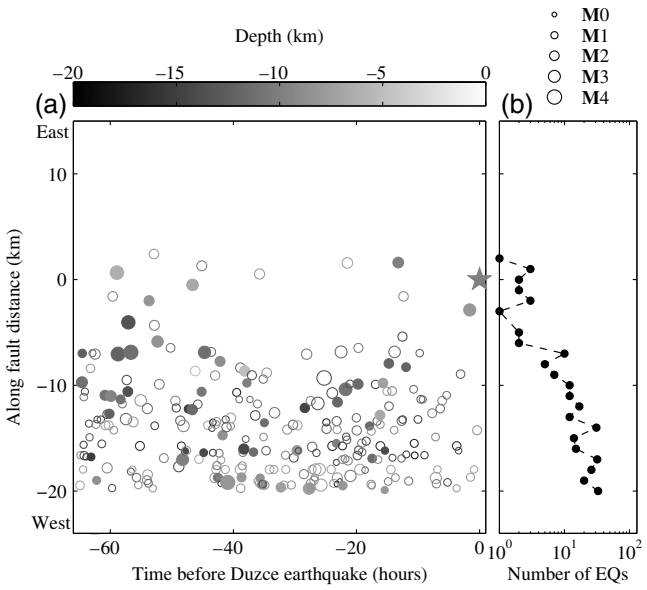

Figure 4. (a) Temporal evolution of foreshock activities along the NAF. The x axis is the time before the Düzce mainshock, and the y axis is the distance along the NAF, with positive value to the west and negative number to the east of the Düzce earthquake epicenter. The detected foreshocks are denoted by shaded circles, with gray scale denoting depth and size denoting magnitude. The solid and open circles indicate the detected events that are listed and not listed in the local catalog, respectively. The gray star shows the Düzce mainshock. (b) The foreshock activities along the NAF.

south and in the Düzce basin to the north of the Düzce epicenter.

The seismicity rate around the Düzce source region varies in the range of ~0–10 events per hour in the 65 hour period prior to the Düzce mainshock, with an average rate of ~4 events per hour (Fig. 3c). The seismicity rate peaked at ~40 about 20 hours before the Düzce mainshock and then gradually dropped to a low value of several events per hour immediately before the Düzce mainshock (Fig. 3c). The spatiotemporal variations of the seismicity do not show progressive migration toward the hypocenter location (Fig. 4). The most active fault segment is at ~10–20 km to the west of the Düzce earthquake epicenter, with an event rate of ~20 events per km during the 65 hour period before the Düzce mainshock. The fault segment at ~0–10 km to the west of the Düzce earthquake epicenter has a seismicity rate of less than 10 events per km, and the fault segment to the east of the Düzce earthquake epicenter has only several events during the 65 hour period.

The results do not indicate evidence for accelerated localizing foreshock activity in the period immediately before the Düzce mainshock (Figs. 3, 4, and S2 Ⓔ available in the electronic supplement to this article). Instead, there are only eight events within 20 km around the Düzce source region during the five hours before the Düzce mainshock, which is well below the average value of 20 events in the earlier five hour periods (Ⓔ Fig. S2, available in the electronic supplement). An examination of temporal changes of the event locations with respect to the Düzce epicenter does not show localized foreshock pattern (Ⓔ Fig. S3, available in the electronic supplement).

Finally, we examine spatiotemporal variations of the seismicity listed in the original catalog (Seeber *et al.*, 2000) in our study region 60 days before to 60 days after the Düzce earthquake (Ⓔ Fig. S4, available in the electronic supplement). Several moderate-size earthquakes occurred a few days before the Düzce mainshock, including an M_w 4.9 earthquake on the Karadere segment on 7 November 1999 and an M_w 5.6 earthquake near Lake Sapanca on 11 November 1999. These events were likely aftershocks of the Izmit mainshock, and each was followed by its own aftershocks (Ⓔ Fig. S4a, available in the electronic supplement). The seismicity around the epicenter of the Düzce mainshock (within 20 km radius) also increased ~40 days before the mainshock and immediately after the M_w 4.9 Karadere earthquake (Ⓔ Fig. S5a, available in the electronic supplement). These events close to the Düzce source region could perhaps

be referred to as foreshocks of the Düzce event. However, our newly detected events within the last 65 hours before the Düzce mainshock did not show any space–time migrations leading to accelerating localizing pattern. Instead, the occurrence rate of the events slowed down right before the Düzce mainshock (Fig. 3c). There are four detected events in the last three hours with magnitudes ranging from ~0 to 1.5 (Ⓔ Fig. S6 available in the electronic supplement to this article), but this is not significant because similar activity occurred at other times before the mainshock.

Discussion

We detected 262 additional earthquakes around the Düzce source region during the 65 hours before the Düzce mainshock. In comparison, only 55 earthquakes were listed in the local catalog at the same time (Seeber *et al.*, 2000). The observed seismicity varies at different segments of the NAF during the 65 hour period. The most active fault segment at ~10–20 km to the west of the Düzce epicenter is bounded by the east termination of the Izmit earthquake rupture (Fig. 1b), so the higher seismicity rate could at least partially be explained as aftershocks of the Izmit earthquake (Ozalaybey *et al.*, 2002). The 10 km fault segment to the west of the Düzce epicenter has a slightly higher seismic activity than the 10 km fault segment to the east (Fig. 4b). This observation is compatible with the background seismicity rate of ~60 days before the Düzce earthquake along the two fault segments (Ⓔ Fig. S4 available in the electronic supplement).

The background seismicity rate at the 10 km fault segment to the west of the Düzce epicenter is much higher than that to the east. One may argue that the spatial variation of the detected events might be due to uneven distribution of template events along the fault. However, we have a similar number of template events at the 10 km fault segments to the east and west of the Düzce epicenter (Ⓔ Fig. S7b available in the electronic supplement), as we also include the aftershocks of the Düzce earthquake as templates. The lack of station coverage may reduce the recording of smaller earthquakes to the east of the Düzce epicenter, but aftershocks to the east of the Düzce epicenter as small as **M** 0.6 were recorded by most of our stations. Hence, the uneven distribution of template events and stations is not likely to have a dominating effect on the observed pattern of the detected events.

Our results as shown in Figures 3 and 4 do not indicate spatiotemporal evolution of seismicity consistent with progressive acceleration and localization within the last 65 hours before the Düzce mainshock. In contrast, the occurrence rate of events appeared to have slowed down right before the Düzce mainshock. Our results and those of other recent studies (West, 2011; Doi and Kawakata, 2012; Peng *et al.*, 2013) indicate that accelerating localizing activity of the type suggested by some theoretical models (Scholz, 1968; Ohnaka and Shen, 1999) and observations (Bouchon *et al.*, 2011; Kato *et al.*, 2012) does not occur generally. Recently, Bouchon *et al.* (2013) investigated foreshocks of 62 **M** > 6.5 earthquakes around the North Pacific, and they suggested that 80% of investigated interplate earthquakes are preceded by accelerated foreshock activity in the months to days before the mainshock. In this study we also find increase of seismicity in the Düzce source region at ~40 days before the mainshock and after the M_w 4.9 Karadere earthquake (Ⓔ Fig. S5a, available in the electronic supplement). However, this involves a broad region rather than the immediate vicinity of the Düzce mainshock location where a decelerating pattern is observed.

Bouchon and Karabulut (2002) examined the seismic recording from a temporary four-station array installed ~five hours before the Düzce mainshock along the Karadere segment, close to our stations VO and FP (Fig. 1). They identified six earthquakes with possible locations in the Düzce source region and estimated local magnitudes from 0.9 to 2.6. Because the four stations of Bouchon and Karabulut (2002) were closely spaced and some of the earthquakes are recorded by less than three stations, they were not able to obtain the location and accurate origin time of the six earthquakes. In our study we detected eight earthquakes in the five hours prior to the Düzce mainshock, including one event listed in the local catalog (Seeber *et al.*, 2000). The estimated magnitudes of these eight detected earthquakes range from 0 to 2.1, indicating that the matched-filter technique utilized in this study can help to identify smaller events from the waveform data. However, only the largest **M** 2.6 event found by Bouchon and Karabulut (2002) was listed in the local catalog as an **M** 2.1 earthquake and is detected in this work.

To investigate why the other five foreshocks of Bouchon and Karabulut (2002) are not detected in this study, we compared the recorded times of the six foreshocks in Bouchon and Karabulut (2002) with our original and selected target waveforms. We found that our network did not record the **M** 2.5, **M** 1.1, and **M** 0.9 events in Bouchon and Karabulut (2002). Our network did record the **M** 1.8 and **M** 1.5 foreshocks of Bouchon and Karabulut (2002), but their recordings did not satisfy the criterion for the target waveforms (recorded by at least four stations) and hence were not detected in this study. We did not include the data used in Bouchon and Karabulut (2002) in the matched-filter analysis because the four stations of Bouchon and Karabulut (2002) are very close in locations (Fig. 1) and do not have the same template events as the 10-station network utilized in this study.

The matched-filter technique has been mostly applied to continuous seismic recordings to detect hidden events (e.g., Peng and Zhao, 2009; Meng *et al.*, 2012, 2013). This study is one of our first attempts to utilize the technique using seismic waveforms recorded in triggered mode. We note the total duration of the triggered recordings within the 65 hour period before the Düzce mainshock is only ~6 hours (or ~1/10 of the total time duration), but the recordings in triggered mode should be able to capture most of the seismic signals above the triggering threshold. To verify this, we examined the total

number of recordings per hour by our network in the 65 hour period (Ⓔ Fig. S1b, available in the electronic supplement). The total number of recordings showed some fluctuations between 40 and 20 hours before the mainshock, and the numbers reduced slightly in the last five hours before the mainshock. We also investigated the peak ground velocity (PGV) of all the vertical-component waveform traces at each station in the 65 hour period, and the PGVs also reduced slightly in the last five hours. Hence, the slight reduction in the numbers of recordings immediately before the mainshock is most likely due to their lower PGVs and magnitudes, rather than missing events with similar PGVs/magnitudes at earlier times. It is possible we may have missed some events with relatively weaker signal or too far from our network due to the recording in triggered mode. However, the observed gradual reduction of seismic activity right before the Düzce mainshock was not likely caused by missing waveform recording and/or changing behaviors in the triggering mode.

In summary, we detected ∼5 times more events than those listed in the standard catalog (Fig. 3). The results suggest that a large portion of events may be missed with standard detection algorithms and that the matched-filter waveform correlation technique could help detect missing events even with seismic recordings in triggered mode. In a future work we plan to apply this technique to the entire dataset recorded by our temporal deployment during its six month operational period. This will require more computation power and efficiency than the current study but will hopefully improve the understanding of the seismicity patterns before and after the Düzce earthquake.

Data and Resources

The seismic data utilized in this study was collected by the Turkey RAMP experiment and can be downloaded from the Incorporated Research Institutions for Seismology Data Management Center (IRIS DMC) (http://www.iris.edu/mda/YJ?timewindow=1999-2000, last accessed February 2013).

Acknowledgments

We thank IRIS DMC for providing the triggered mode seismic data in the last three days right before the Düzce mainshock. The manuscript benefited from useful comments by Michael West and Associate Editor Heather DeShon. The study was supported by the National Science Foundation Grants EAR-0956051, EAR-1321550 (C. W., X. M., Z. P.), and EAR-1141944 (Y. B. Z.).

References

Abercrombie, R. E., and J. Mori (1996). Occurrence patterns of foreshocks to large earthquakes in the western United States, *Nature* **381,** 303–307.

Ben-Zion, Y. (2008). Collective behavior of earthquakes and faults: Continuum-discrete transitions, progressive evolutionary changes, and different dynamic regimes, *Rev. Geophys.* **46,** no. 4, RG4006, doi: 10.1029/2008RG000260.

Ben-Zion, Y., Z. Peng, D. Okaya, L. Seeber, J. Armbruster, N. Ozer, A. Michael, S. Baris, and M. Aktar (2003). A shallow fault-zone structure illuminated by trapped waves in the Karadere-Düzce branch of the North Anatolian Fault, western Turkey, *Geophys. J. Int.* **152,** no. 3, 699–717.

Bouchon, M., and H. Karabulut (2002). A note on seismic activity near the eastern termination of the Izmit rupture in the hours preceding the Düzce earthquake, *Bull. Seismol. Soc. Am.* **92,** no. 1, 406.

Bouchon, M., V. Durand, D. Marsan, H. Karabulut, and J. Schmittbuhl (2013). The long precursory phase of most large interplate earthquakes, *Nature Geosci.* **6,** no. 4, 299–302.

Bouchon, M., H. Karabulut, M. Aktar, S. Özalaybey, J. Schmittbuhl, and M. P. Bouin (2011). Extended Nucleation of the 1999 M_w 7.6 Izmit Earthquake, *Science* **331,** no. 6019, 877.

Chen, X., and P. M. Shearer (2013). California foreshock sequences suggest aseismic triggering process, *Geophys. Res. Lett.* **40,** 2602–2607, doi: 10.1002/grl.50444.

Dodge, D. A., G. C. Beroza, and W. Ellsworth (1995). Foreshock sequence of the 1992 Landers, California, earthquake and its implications for earthquake nucleation, *J. Geophys. Res.* **100,** no. B6, 9865–9880.

Dodge, D. A., G. C. Beroza, and W. Ellsworth (1996). Detailed observations of California foreshock sequences: Implications for the earthquake initiation process, *J. Geophys. Res.* **1012,** 22,371–22,392.

Doi, I., and H. Kawakata (2012). A non-accelerating foreshock sequence followed by a short period of quiescence for a large inland earthquake, *Geophys. Res. Lett.* **39,** no. 11, L11308, doi: 10.1029/2012GL051779.

Jones, L. M., and P. Molnar (1979). Some characteristics of foreshocks and their possible relationship to earthquake prediction and premonitory slip on faults, *J. Geophys. Res.* **84,** no. B7, 3596–3608.

Kato, A., K. Obara, T. Igarashi, H. Tsuruoka, S. Nakagawa, and N. Hirata (2012). Propagation of slow slip leading up to the 2011 M_w 9.0 Tohoku-Oki earthquake, *Science* **335,** no. 6069, 705–708.

Meng, X., Z. Peng, and J. Hardebeck (2013). Seismicity around Parkfield correlates with static shear stress changes following the 2003 M_w 6.5 San Simeon earthquake, *J. Geophys. Res* **118,** 1–16, doi: 10.1002/jgrb.50271.

Meng, X., X. Yu, Z. Peng, and B. Hong (2012). Detecting earthquakes around Salton Sea following the 2010 M_w 7. 2 El Mayor-Cucapah earthquake using GPU parallel computing, *Procedia Comp. Sci.* **9,** 937–946.

Ohnaka, M., and L. Shen (1999). Scaling of the shear rupture process from nucleation to dynamic propagation: Implications of geometric irregularity of the rupturing surfaces, *J. Geophys. Res* **104,** no. B1, 817–844.

Ozalaybey, S., M. Ergin, M. Aktar, C. Tapirdamaz, F. Bicmen, and A. Yoryk (2002). The 1999 Izmit earthquake sequence in Turkey: Seismological and tectonic aspects, *Bull. Seismol. Soc. Am.* **92,** no. 1, 376–386.

Peng, Z., and P. Zhao (2009). Migration of early aftershocks following the 2004 Parkfield earthquake, *Nature Geosci.* **2,** no. 12, 877–881.

Peng, Z., B. Wang, and H. Tu (2013). Immediate foreshock activity of the 2010 M_w 6.9 Yushu, Qinghai earthquake, *Abstract submitted to the 2013 Annual Seismological Society of America Meeting*, Salt Lake City, Utah, 17–19 April 2013.

Scholz, C. (1968). The frequency-magnitude relation of microfracturing in rock and its relation to earthquakes, *Bull. Seismol. Soc. Am.* **58,** no. 1, 399–415.

Seeber, L., J. Armbruster, N. Ozer, M. Aktar, S. Baris, D. Okaya, Y. Ben-Zion, and E. Field (2000). The 1999 Earthquake Sequence along the North Anatolia Transform at the juncture between the two main ruptures, in *The 1999 Izmit and Düzce Earthquakes: Preliminary Results*, A. Barka, O. Kozaci, S. Akyuz, and E. Altunel (Editors), no. 209–223, Istanbul Technical University, Turkey.

Shelly, D., G. Beroza, and S. Ide (2007). Non-volcanic tremor and low-frequency earthquake swarms, *Nature* **446,** no. 7133, 305–307.

West, M. (2011). No evidence of slow slip microearthquakes prior to 2002 Denali Fault earthquake, *Abstract submitted to the 2011 Earthscope National Meeting*, Austin, Texas, 17–20 May 2011.

Zaliapin, I., and Y. Ben-Zion (2013a). Earthquake clusters in southern California II: Classification and relation to physical properties of the crust, *J. Geophys. Res.* **118,** doi: 10.1002/jgrb.50178.

Zaliapin, I., and Y. Ben-Zion (2013b). Earthquake clusters in southern California I: Identification and stability, *J. Geophys. Res.* **118,** doi: 10.1002/jgrb.50179.

Zanzerkia, E. E., G. C. Beroza, and J. E. Vidale (2003). Waveform analysis of the 1999 Hector Mine foreshock sequence, *Geophys. Res. Lett.* **30,** no. 8, 1429.

Geophysics Group
Los Alamos National Laboratory
Los Alamos, New Mexico 87545
cwu@lanl.gov
(C.W.)

School of Earth and Atmospheric Sciences
Georgia Institute of Technology
Atlanta, Georgia 30332
(X.M., Z.P.)

Department of Earth Sciences
University of Southern California
Los Angeles, California 90089
(Y.B.-Z.)

Manuscript received 30 May 2013;
Published Online 10 December 2013

Supp. Figure Captions

Figure S1. (a) Timing of the recorded waveforms at the 10 stations during the 65 hours before the Duzce main shock. The station names are listed on the left and the numbers of triggered recordings are listed on the right. The blue and red vertical lines at the top show the timing the earthquakes listed in the local catalog (Seeber *et al.*, 2000) and six foreshocks of Duzce earthquake identified by Bouchon and Karabulut (2002). Note that the 4th red lines overlaps with a blue line so only the red line could be seen. (b) Total number of recordings by the 10 stations in each hour of the 65 hours before the Duzce main shock. The horizontal red dashed line shows the average number of recordings per hour. (c) Peak ground velocities (PGVs) of all the vertical-component recordings during the 65 hours before the Duzce main shock.

Figure S2. Histogram of the detected foreshock activities along the NAF in every 5 hours within the last 65 hours before the Duzce main shock.

Figure S3. (a) Temporal pattern of foreshock activities in different distance ranges to the Duzce earthquake epicenter. X-axis is the time before the Duzce main shock in hours, and Y-axis is the distance to Duzce earthquake epicenter in km. The detected foreshocks are denoted by shaded circles with grey scale denoting depth, and size denoting magnitude. The grey star shows the Duzce main shock. (b) Histogram of the seismicity rate (number/km^2) in different distance ranges to the Duzce

earthquake epicenter.

Figure S4. (a) Daily seismicity rate from the local catalog (Seeber *et al.*, 2000) within ~100 km to the Duzce epicenter in the period from 60 days before to 60 days after the Duzce earthquake. The three vertical red dashed lines indicate the occurrence time the Mw5.6 Sapanca earthquake, Mw4.9 Karadere earthquake, and the Mw7.1 Duzce earthquake, respectively. (b) Temporal evolutions of earthquake activities listed in the catalog within the region from -100 to 50 km along the NAF. X-axis is the time before the Duzce main shock in hours, and Y-axis is the distance along the NAF in km, with positive value to the East and negative number to the West of the Duzce earthquake epicenter. The M<4 earthquakes are shown in small black dots, and the M>4 earthquakes are shown in large red circles with size denoting magnitude. The red star shows the Duzce main shock. (c) Histogram of the earthquake activities along the NAF.

Figure S5. Similar figure as Figure S4 for events within ~20 km of the Duzce epicenter.

Figure S6. Vertical component of the target waveforms recorded by FP and nearby stations within 3 hours before the Duzce main shock. The time in seconds before the Duzce main shock is marked on the left and the station is marked on the right. The vertical red bars mark the origin time of the 4 detected Duzce foreshocks. The

template waveforms for the 4 detections are shown in red with the CC value by its side. The onset of the Duzce main shock is marked by the red arrow under the bottom trace.

Figure S7. (a) Distribution of the template events along the North Anatolian fault (NAF). X-axis is the time before the Duzce main shock in hours, and Y-axis is the distance along the NAF in km, with positive value to the east and negative number to the west of the Duzce earthquake epicenter. The template events are denoted by shaded circles with grey scale denoting depth, and size denoting magnitude. The grey star shows the Duzce main shock. (b) Histogram of the template events along the NAF.

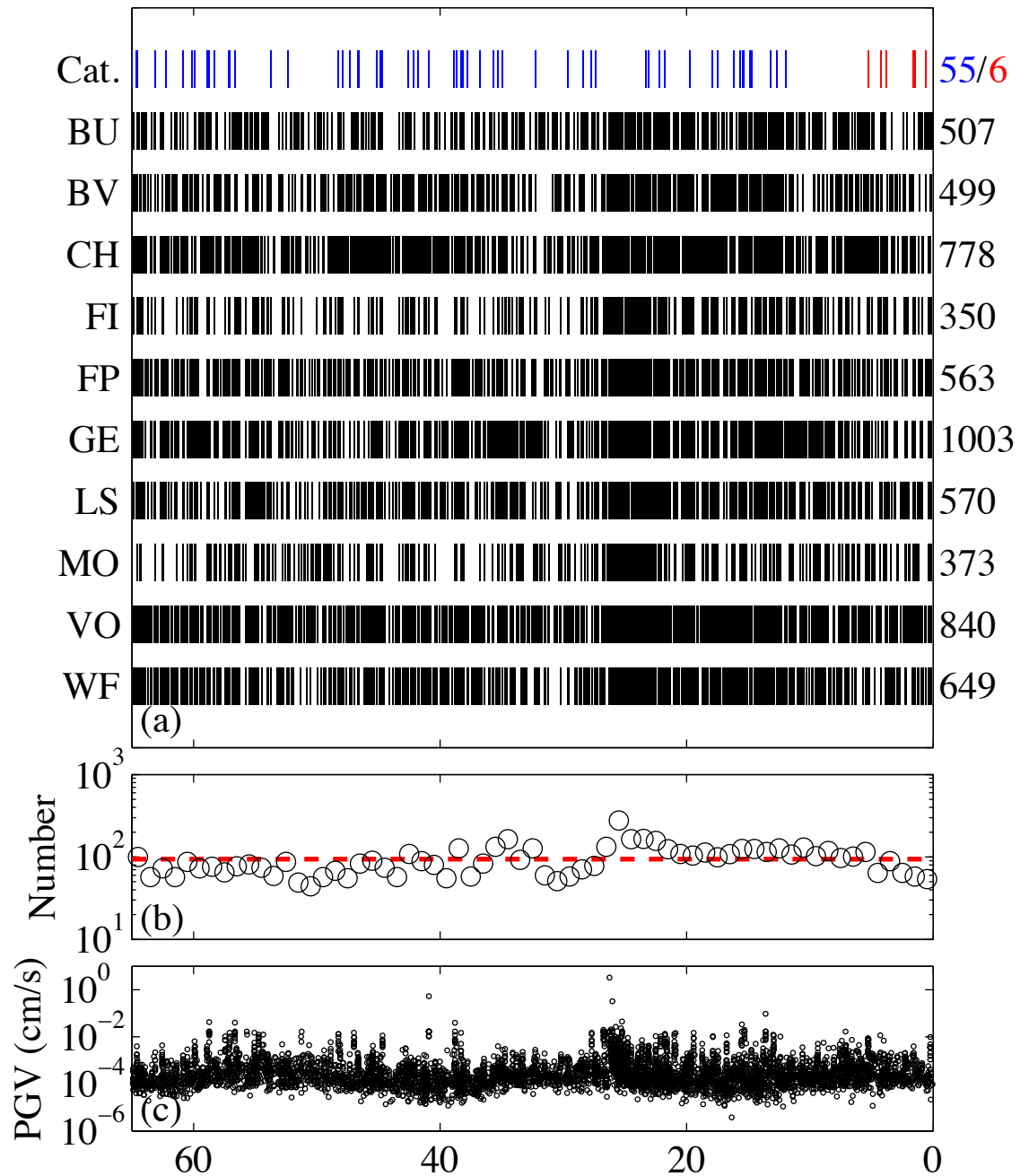
Cat.
55/6
BU
507
BV
499
CH
778
FI
350
FP
563
GE
1003
LS
570
MO
373
VO
840
WF
649
(a)
Number
(b)
PGV (cm/s)
(c)
60
40
20
0
Hours before the Duzce earthquake

Figure S1

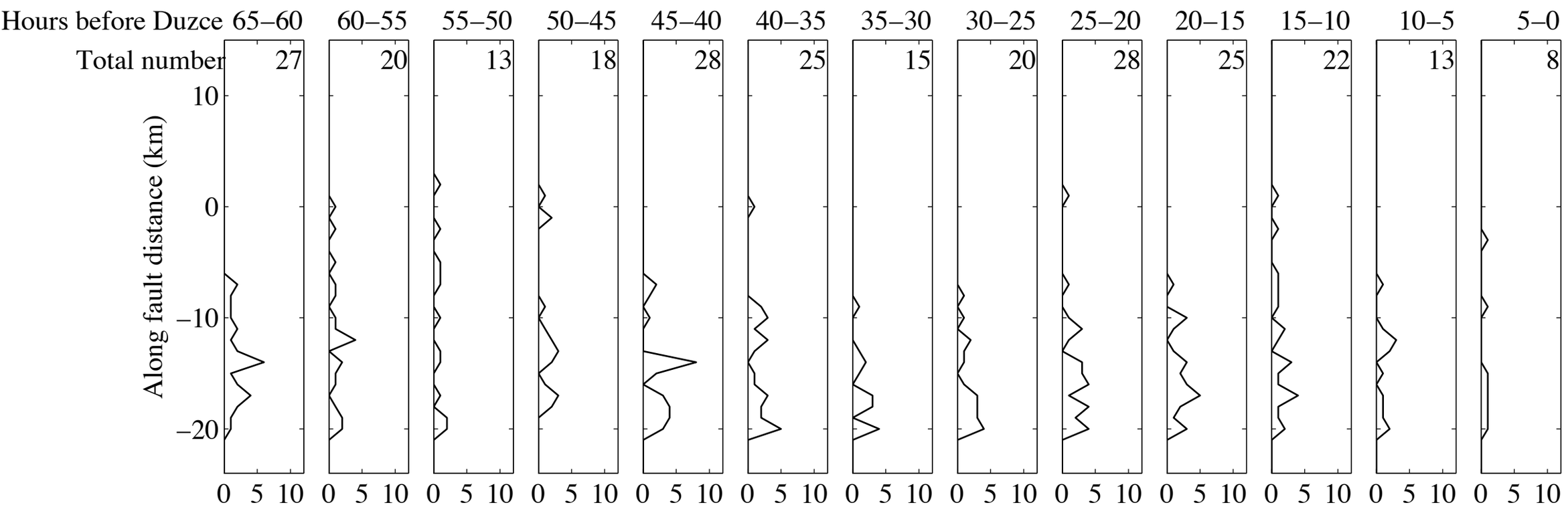
Hours before Duzce
65–60
60–55
55–50
50–45
45–40
40–35
35–30
30–25
25–20
20–15
15–10
10–5
5–0
Total number
27
20
13
18
28
25
15
20
28
25
22
13
8
Along fault distance (km)
10
0
−10
−20
0 5 10
Number of earthquakes

Figure S2

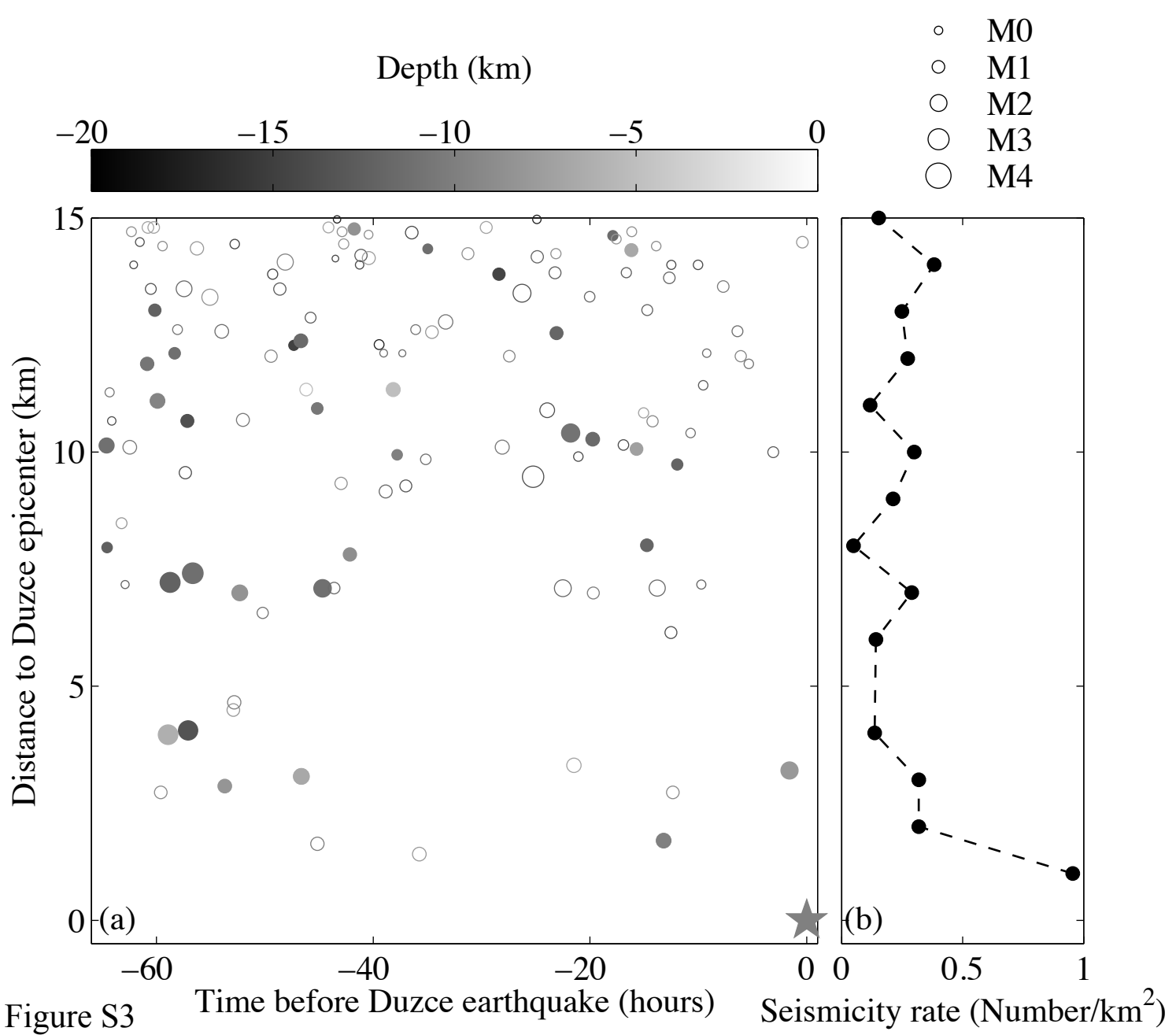
Depth (km)
−20
−15
−10
−5
0
M0
M1
M2
M3
M4
15
10
5
0
Distance to Duzce epicenter (km)
(a)
(b)
−60
−40
−20
0
Time before Duzce earthquake (hours)
0
0.5
1
Seismicity rate (Number/km^2)

Figure S3

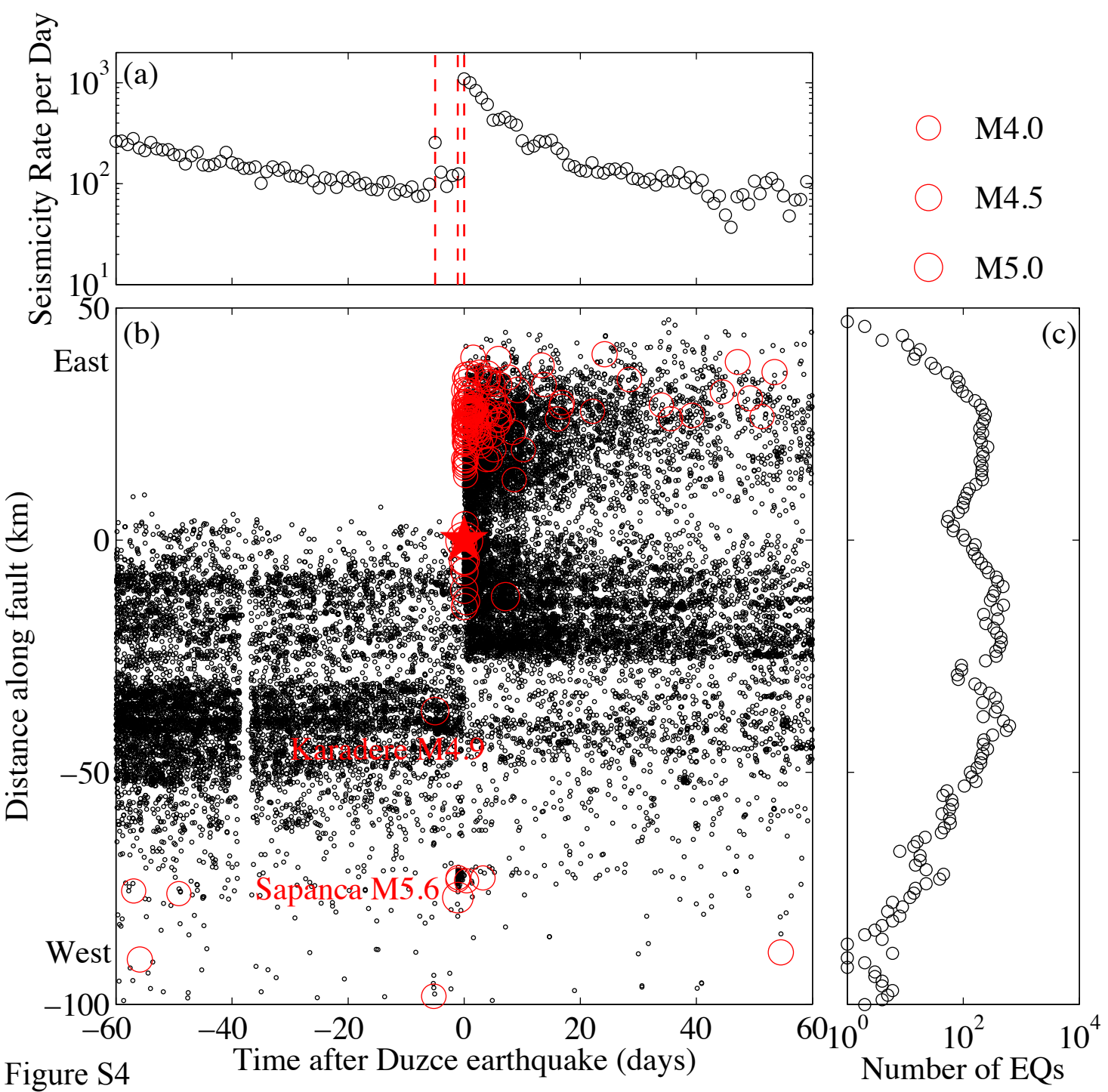
(a)
Seismicity Rate per Day
10^3
10^2
10^1
M4.0
M4.5
M5.0
(b)
East
West
50
0
−50
−100
Distance along fault (km)
Karadere M7.9
Sapanca M5.6
−60
−40
−20
0
20
40
60
Time after Duzce earthquake (days)
(c)
10^0
10^2
10^4
Number of EQs

Figure S4

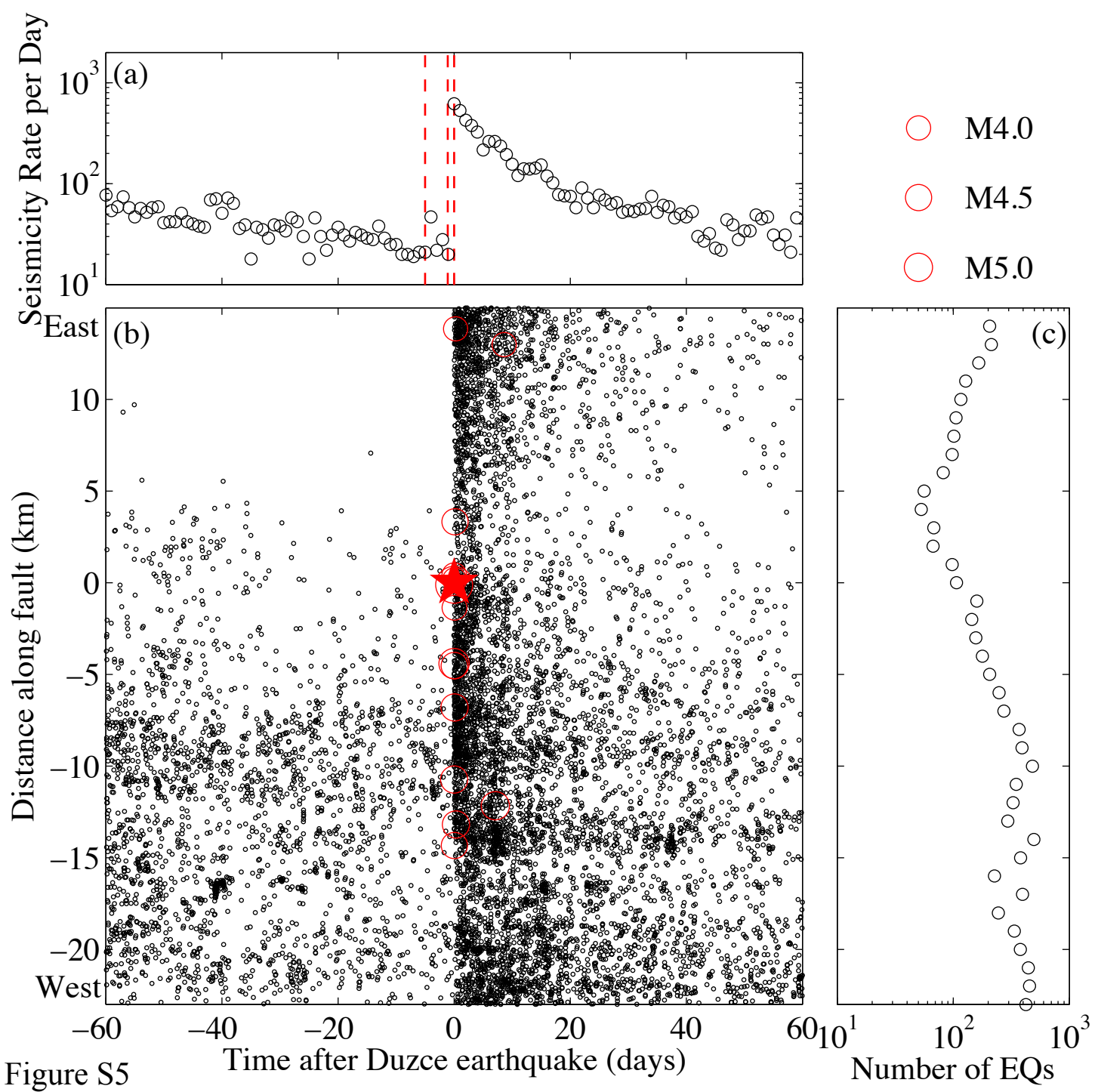
(a)
(b)
(c)
Seismicity Rate per Day
10^3
10^2
10^1
M4.0
M4.5
M5.0
East
West
Distance along fault (km)
10
5
0
−5
−10
−15
−20
−60
−40
−20
0
20
40
60
Time after Duzce earthquake (days)
10^1
10^2
10^3
Number of EQs

Figure S5

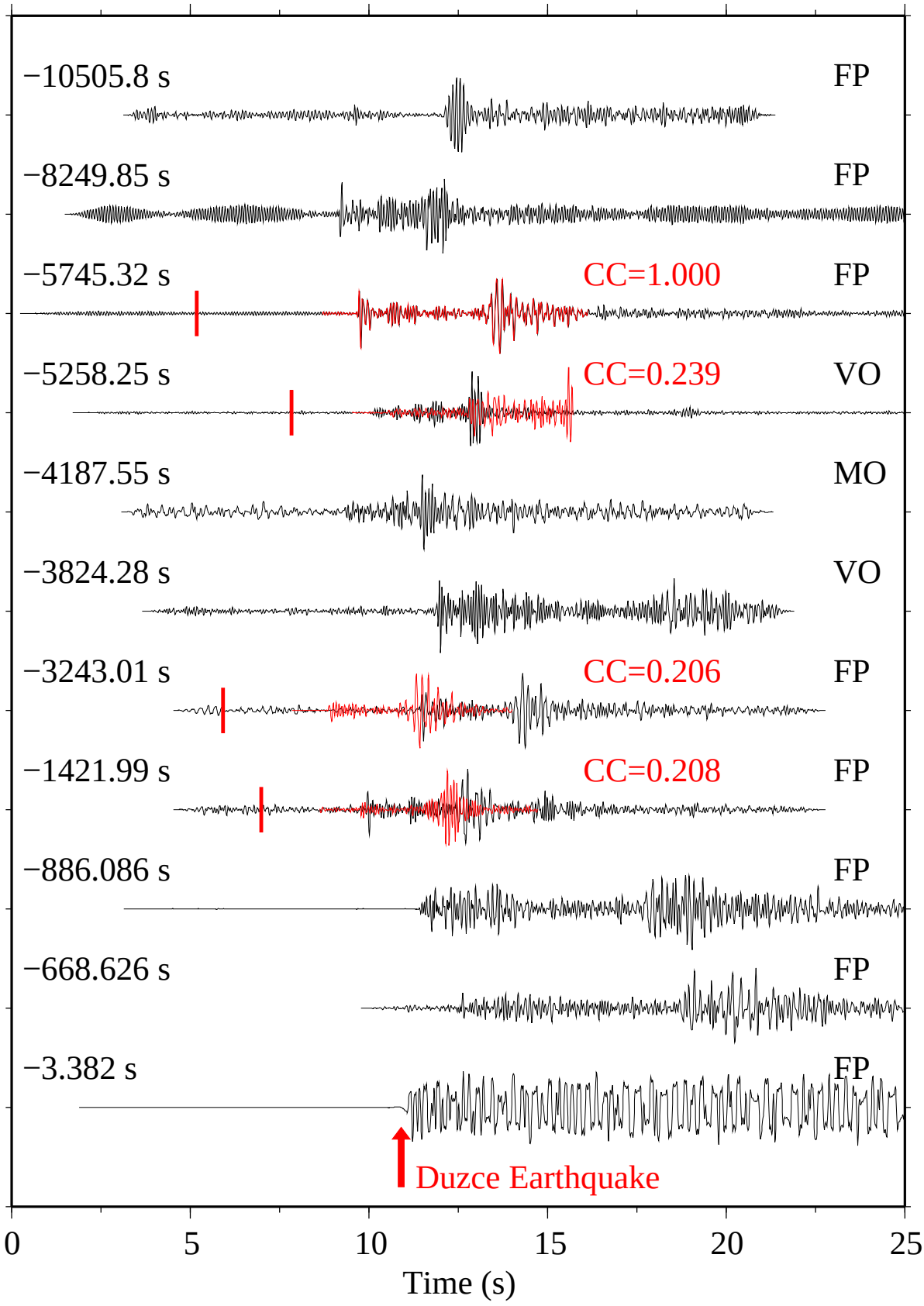
−10505.8 s
FP
−8249.85 s
FP
−5745.32 s
CC=1.000
FP
−5258.25 s
CC=0.239
VO
−4187.55 s
MO
−3824.28 s
VO
−3243.01 s
CC=0.206
FP
−1421.99 s
CC=0.208
FP
−886.086 s
FP
−668.626 s
FP
−3.382 s
FP
Duzce Earthquake
0
5
10
15
20
25
Time (s)

Figure S6

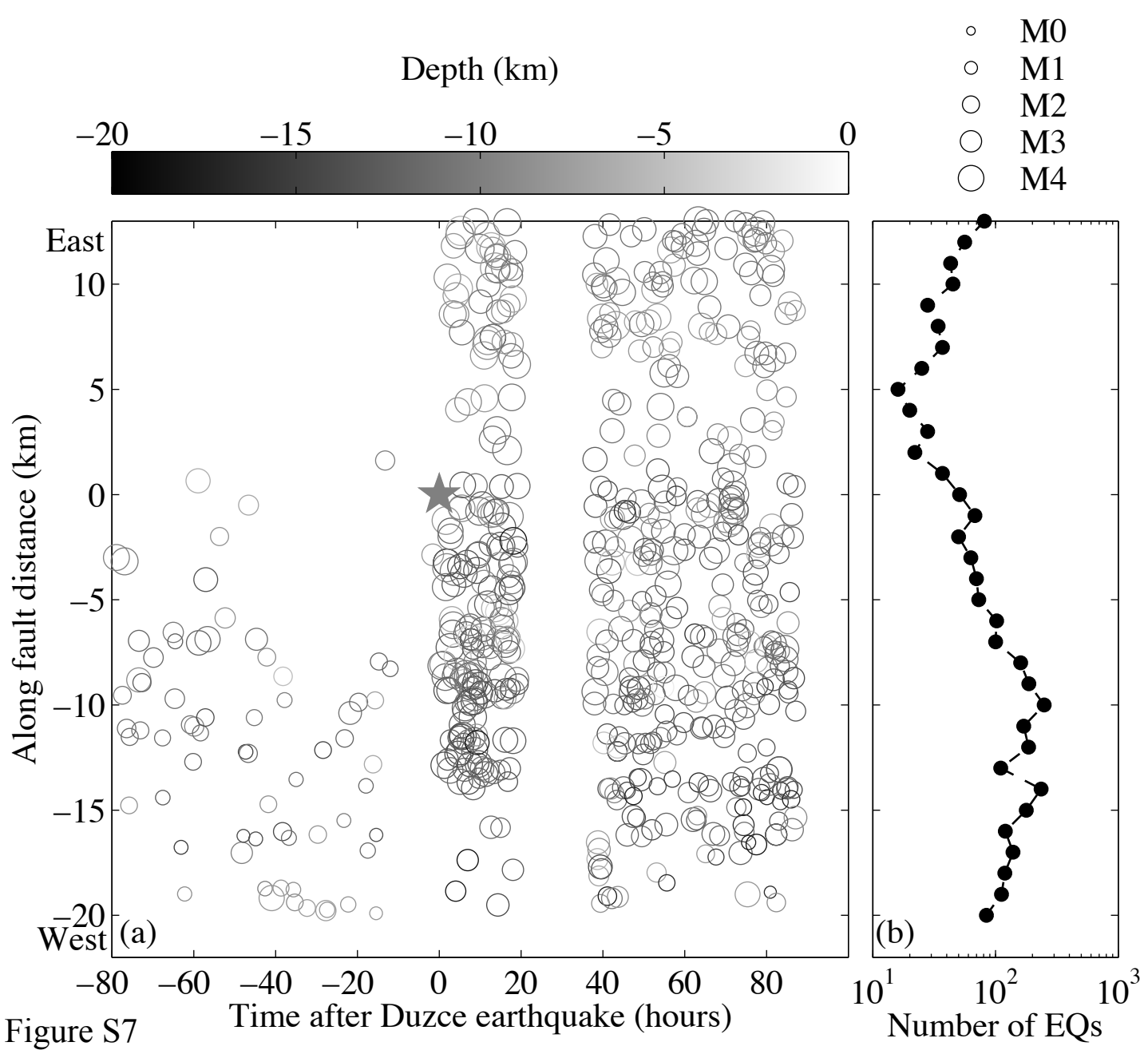
Depth (km)
−20
−15
−10
−5
0
M0
M1
M2
M3
M4
East
West
Along fault distance (km)
10
5
0
−5
−10
−15
−20
(a)
(b)
−80
−60
−40
−20
0
20
40
60
80
Time after Duzce earthquake (hours)
10^1
10^2
10^3
Number of EQs

Figure S7